LAWRENCE
LIVERMORE
NATIONAL
LABORATORY

UCRL-JRNL-206523

In Vitro Fracture of Human Cortical Bone: Local Fracture Criteria and Toughening Mechanisms

R. K. Nalla, J.S. Stolken, J. H. Kinney and R. O. Ritchie

September 2004

This work was performed under the auspices of the U. S. Department of Energy by the University of California, Lawrence Livermore National Laboratory under Contract No. W-7405-Eng-48.

This document was prepared as an account of work sponsored by an agency of the United States Government. Neither the United States Government nor the University of California nor any of their employees, makes any warranty, express or implied, or assumes any legal liability or responsibility for the accuracy, completeness, or usefulness of any information, apparatus, product, or process disclosed, or represents that its use would not infringe privately owned rights. Reference herein to any specific commercial product, process, or service by trade name, trademark, manufacturer, or otherwise, does not necessarily constitute or imply its endorsement, recommendation, or favoring by the United States Government or the University of California. The views and opinions of authors expressed herein do not necessarily state or reflect those of the United States Government or the University of California, and shall not be used for advertising or product endorsement purposes.

01/28/03-11:11 AM
Report No. LBNL-51910

Materials Sciences Division, Lawrence Berkeley National Laboratory, and
Department of Materials Science and Engineering
University of California at Berkeley

IN VITRO FRACTURE OF HUMAN CORTICAL BONE: LOCAL FRACTURE CRITERIA AND TOUGHENING MECHANISMS

***R. K. Nalla*[1], *J. S. Stölken*[2], *J. H. Kinney*[2] *and R. O. Ritchie*[1,3]**

[1] Materials Sciences Division, Lawrence Berkeley National Laboratory, and
Department of Materials Science and Engineering,
University of California, Berkeley, CA 94720

[2] Lawrence Livermore National Laboratory,
Livermore, CA 94550

[3] Corresponding author:
Department of Materials Science and Engineering,
381 Hearst Mining Building,
University of California, Berkeley, CA 94720-1760

Tel: (510) 486-5798; Fax: (510) 486-4881
E-mail address: RORitchie@lbl.gov (R. O. Ritchie)

January 2003

Original Article submitted to *Journal of Biomechanics*

Total word count: 4,910 (Introduction through Discussion)

This work was supported in part by the National Institutes of Health under Grant No. P01DE09859 (for RKN and JHK), and by the Director, Office of Science, Office of Basic Energy Science, Division of Materials Sciences and Engineering of the Department of Energy under Contract No. DE-Ac03-76SF00098 (for ROR).

On the Micro-Mechanisms of *In Vitro* Fracture and Toughening in Human Cortical Bone

R. K. Nalla[1], J. S. Stölken[2], J. H. Kinney[2] and R. O. Ritchie[1]

[1]Materials Sciences Division, Lawrence Berkeley National Laboratory, and Department of Materials Science and Engineering, University of California, Berkeley, CA 94720

[2]Lawrence Livermore National Laboratory, Livermore, CA 94550

Abstract

A micro-mechanistic understanding of bone fracture that encompasses how cracks interact with the underlying microstructure and defines their *local* failure mode is lacking, despite extensive research on the response of bone to a variety of factors like aging, loading, and/or disease. Micro-mechanical models for fracture incorporating such local failure criteria have been widely developed for metallic and ceramic materials systems; however, few such deliberations have been undertaken for the fracture of bone. In fact, although the fracture event in mineralized tissues such as bone is commonly believed to be locally strain-controlled, until recently there has been little experimental evidence to support this widely held belief. In the present study, a series of *in vitro* experiments involving a double-notch bend test geometry are performed in order to shed further light on the nature of the local cracking events that precede catastrophic fracture in bone and to define their relationship to the microstructure. Specifically, crack-microstructure interactions are examined to determine the salient toughening mechanisms in human cortical bone and to characterize how these may affect the anisotropy in fracture properties. Based on preliminary micro-mechanical models of these processes, in particular crack deflection and uncracked ligament bridging, the relative importance of these toughening mechanisms is established.

Keywords: Bone, fracture, toughening, microstructure.

1. Introduction

Over the past few decades, interest in bone and its mechanical properties has led to extensive research into how it fractures (e.g., Lindahl and Lindgren, 1967; Currey, 1970; Burnstein et al., 1976; Wright and Hayes, 1976; Katz, 1980; Ashman and Rho, 1988; Park and Lakes, 1992; Keaveny et al., 1993; Vashishth at al., 1997; Zioupus and Currey, 1998; Burr, 2002; Nalla et al., 2003(1)). Nevertheless, many fundamental questions remain to be addressed. For example, although the critical fracture event in bone is widely believed to be *locally* strain-controlled and models for bone fracture are invariably based on this concept (e.g., Keaveny et al., 1994; Ford and Keaveny, 1996; Yeh and Keaveny, 2001), until recently (Nalla et al., 2003(1)), there has been little to no direct experimental evidence to verify this hypothesis. Moreover, current micro-mechanical models for *in vitro* bone fracture generally fail to capture the interaction of the crack with the salient microstructural features at the various characteristic length scales, which in turn leads to the development of toughening; indeed, a detailed description of the origins of the toughness of bone is as yet incomplete.

Recently, we used a double-notch four-point bend geometry to obtain the first direct evidence that fracture is bone is consistent with a locally strain-based criterion (Nalla et al., 2003(1)). The prime objective of the present work is to seek further understanding of the factors that contribute to the fracture properties of human cortical bone by examining the local failure events for the onset of cracking and, by identifying the salient toughening mechanisms, to discern how the subsequent crack growth is affected by the microstructure.

Various toughening mechanisms have been proposed for bone (Vashishth at al., 1997; Burr, 2002; Vashishth, 2000; Parsamian and Norman, 2001; Vashishth et al., 2000; Yeni and Norman, 2000; Wang et al., 2001; Thompson et al., 2001; Wang et al., 2002; Yeni and

Fyhrie, 2001), although in many cases with little experimental and/or theoretical verification. At the largest length scales, the generation of microcracks (so-called "microdamage") in the vicinity of the crack tip (Vashishth at al., 1997; Vashishth, 2000; Parsamian and Norman, 2001; Vashishth et al., 2000) is believed to contribute to the fracture toughness, specifically via crack-tip shielding, although this mechanism, in general, is not a particularly potent toughening mechanism. In addition, the cement lines at the boundaries of the (secondary) osteons are believed to provide weak interfaces that deflect the crack path, thereby increasing the toughness (Yeni and Norman, 2000). More recently, a role of the mineralised collagen fibrils has been identified (Wang et al., 2001; Thompson et al., 2001; Wang et al., 2002), and a fiber-bridging model proposed as a possible toughening mechanism (Yeni and Fyhrie, 2001). Toughening at the fibrilar level would explain much of the apparent correlation of toughness with collagen denaturation, which appears to weaken bone, and cross-links, which appear to increase its toughness (Burr, 2002). Unfortunately, little definitive information exists for the potency of these toughening mechanisms; moreover, it is probable that they operate *in concert*, depending on the orientation of the crack with respect to the microstructure. In the present study, we seek to enumerate such possibilities in the context of the role of microstructure in affecting the orientation dependence of the fracture toughness of cortical bone, and where possible, to quantify the effect of the various micro-mechanisms involved by both experimental measurement and theoretical modeling.

2. Materials and Methods

Qualitatively, local events that result in macroscopic fracture can be described as either locally *stress*- or *strain-controlled*. This is an important distinction in understanding the

nature of fracture from a sharp crack or rounded notch because, as described in the Appendix, in the presence of any degree of inelasticity, e.g., plastic deformation or microcracking, the maximum local plastic strains are located *at* the crack or notch tip whereas the local tensile stresses are at a maximum some distance *ahead* of the tip (e.g., Fig. 1). This phenomenon has recently been exploited to examine failure both in bone (Nalla et al., 2003(1)) and dentin (Nalla et al., 2003(2)).

As described in Nalla et al., 2003(1), insight into the distinction between stress- and strain-controlled fracture can be obtained using a double-notched four-point bend geometry (Fig. 2). This test sample contains rounded notches with a large root radius ($\rho \sim 200$-300 μm) in order to maximize the difference between the locations of maximum stress and strain; the maximum strains are at the notch root and decrease monotonically with distance ahead of the notch, whereas the maximum stresses are ahead of the notch closer to the elastic/inelastic interface (Griffiths and Owen, 1971). This sample employs two notches subjected to four-point bending because, as there is a constant bending moment between the inner two loading points, both notches see identical stress and strain states. For a nominally brittle material, such as bone, this means that when unstable fracture ensues from one notch, the other notch will literally be at the point of instability, thereby "freezing in" the local microstructural cracking events that immediately precede fracture. Examination of the microstructure below this unbroken notch thus enables an evaluation of how and where the critical cracking processes initiate, and in doing so define whether the process is stress- or strain-controlled.

2.1 Materials and mechanical testing:

A fresh frozen human cadaveric humerus from a 34-year old female was used in this study. Beams of cortical bone, obtained by carefully sectioning the humerus, were wet

polished down to the final size to a 1200 grit surface finish, followed by a final polishing step using a 0.05 μm alumina paste. Mechanical tests were conducted using a symmetric four-point bending geometry with a double-notched configuration (Fig. 2a); the thickness and width of the samples were, respectively, $B \sim 1.0\text{-}2.7$ mm and $W \sim 2\text{-}3$ mm, with a spacing between the inner loading points of $S \sim 10\text{-}15$ mm. Rounded notches, with a root radius of $\rho \sim 200\text{-}300$ μm and a depth of $a \sim 0.3\text{-}0.4\ W$, were then cut with a slow speed saw. The depths of both notches in each specimen were identically machined in order to ensure similar stress/strain fields at the notch tips. The specimens were maintained in a hydrated state using a physiological solution (Hanks' Balanced Salt Solution, HBSS) throughout all specimen preparation and testing processes.

A total of eighteen tests (N = 18) were conducted, with at least four tests in each orientation investigated (Fig. 3). Specifically, three orientations were examined:

- *Anti-plane longitudinal*, with the long axes of the osteons in the plane of the notch/subsequent crack, but perpendicular to the nominal direction of crack propagation (N = 4),
- *In-plane longitudinal*, with the long axes of the osteons in the plane of the notch/subsequent crack, but perpendicular to the nominal direction of crack propagation (N = 5), and
- *Transverse*, with the long axes of the osteons perpendicular to the plane of the notch/subsequent crack and to the nominal direction of crack propagation (N = 9).

All testing was conducted at ambient temperature in HBSS using an ELF® 3200 series voice coil-based mechanical testing machine (EnduraTEC Inc., Minnetonka, MN). The bend bars

were loaded to failure under displacement control at a constant cross-head displacement rate of 0.01 mm/sec.

3.2 Microstructure/crack path interaction and fractographic observations:

The area around the unfractured notch in the failed double-notched samples (as indicated in Fig. 2b) was examined using a high-power optical microscope and, after coating with a gold-palladium alloy, in a scanning electron microscope (SEM) operating in the back-scattered electron mode. In addition, post-failure observations of the fracture surfaces of the broken ligaments were made using the same techniques.

3.3 Fracture-toughness measurements:

Fracture-toughness K_c testing was performed in general accordance with the ASTM Standard E-399 for Plane-Strain Fracture Toughness. Tests were conducted using the three-point bending geometry (specimen width, W ~ 1.7-2.7 mm and thickness, B ~ 1.1-2.6 mm) with a span between the lower two loading points equal to 5-5.5 times the width of the beam (S = 5-5.5 W) (Fig. 4a). Both longitudinal and transverse orientations (Fig. 3) were investigated (N = 3 for each orientation). A precrack was grown out of the notch by cycling in fatigue; this was achieved at a load ratio (ratio of minimum to maximum loads) of R = 0.1 and loading frequency of 2 Hz, with a final maximum stress intensity of K_{max} ~ 1-2 MPa√m. The final precrack length (notch plus precrack) was generally ~0.4-0.6 W, with a presumed atomically sharp crack tip. Fig. 4b shows an optical micrograph of one such crack emanating from the blunt notch. A fatigue precrack, as opposed to a sharp machined notch, was used in all fracture toughness test samples to eliminate possible notch-radius effects which can erroneously elevated the measured toughness (Imbeni et al., 2003). Samples were loaded to failure under displacement control with an ELF® 3200 series machine at ambient temperature

at a cross-head displacement rate of 0.01 mm/sec in HBSS. The applied loads and the corresponding load-line displacements were simultaneously monitored throughout the test. Three separate specimens were tested for each orientation.

Linear-elastic stress intensities, K, were computed from handbook solutions, specifically from the ASTM Standard E-399 for Plane-Strain Fracture Toughness. For the three-point bending specimen used:

$$K = \left(\frac{P\,S}{B W^{3/2}} \right) f(a/W) \ , \tag{1a}$$

where P is the applied load, S is the distance between the outer loading pins, a is the crack length, B and W are, respectively, the specimen thickness and width (Fig. 4a), and $f(a/W)$ is dimensionless function of a/W given by:

$$f(a/W) = \frac{3(a/W)^{1/2}[1.99-(a/W)(1-(a/W))(2.15-3.93(a/W)+2.7(a/W)^2]}{2(1+2(a/W))(1-(a/W))^{3/2}} \ . \tag{1b}$$

The fracture toughness, K_c, was measured at the point of instability consistent with the onset of unstable fracture. According to ASTM Standard E-399, a state of plane strain is achieved when the sample thickness is greater than 2.5 $(K_c/\sigma_y)^2$, where σ_y is the tensile "yield" stress; this implies that the thickness is significantly larger than the plastic or damage zone size of $r_y \sim 1/2\pi\ (K_c/\sigma_y)^2$. For cortical bone, where we estimate the tensile strength to be on the order of 80 MPa (An, 2000), this would require samples thicknesses greater than approximately 2-11 mm (depending on specimen orientation) to yield a plane-strain K_c value. As this criterion is generally quite conservative and as our observations show the damage zone to be well-contained within the specimen boundaries, it is believed that the toughness values measured

with the current test specimens are very close to the plane-strain value, which represents a lower-bound.

Due to substantial crack deflections for the transverse orientation in bone (see Section 4.2), mode I fracture mechanics parameters such as K_c may be regarded as somewhat specious. Consequently, additional measurements were made of an alternative measure of toughness, the work of fracture, W_f, which was obtained by dividing the area under the load-displacement curve obtained for each test by twice the nominal crack surface area. It should be noted, however, that the work of fracture parameter is both size- and geometry-dependent.

3.4 Crack-bridging experiments:

One proposed mechanism of toughening in bone is crack bridging, by for example collagen fibrils (Yeni and Fyhrie, 2001) or uncracked ligaments (Nalla et al., 2003(1)). To experimentally verify the presence of crack bridging, a crack was grown from a rounded notch (a ~ 1-1.5 mm) in three-point bend specimens (N = 4). The "measured" compliance (inverse stiffness) of this cracked specimen was then determined by monitoring the load-line displacement as a function of the applied bending load. This was then compared to the "theoretical" compliance for a specimen with a traction-free crack of identical length in this geometry obtained from the calculated load-line displacement, δ that is given by (Haggag and Underwood, 1984):

$$\delta = \delta_{bend} + \delta_{shear} + \delta_{crack} \ , \qquad (2)$$

where $\delta_{bend} = PS^3/4B^3E$ is the bending displacement, $\delta_{shear} = 0.6(1+\nu)\ PS/BWE$ is the shear displacement and $\delta_{crack} = 6PS^2f(a/W)/4BW^2E$ is the displacement due to the crack. Here, P is the applied load, S is the loading span, a is the crack length, B and W are, respectively, the

specimen thickness and width, E is the Young's modulus, ν is the Poisson's ratio and $f(a/W)$ is dimensionless function of a/W (Haggag and Underwood, 1984). To check the veracity of the theoretical estimate for the case of bone, the wake of the crack was then carefully machined out using a slow speed diamond saw to obtain a nominally traction-free "crack" of the same length, and the compliance was re-measured. (Note that the width of the machined slot, which was on the order of 300 μm, has no influence on the specimen compliance).

3. Results

3.1 Double-notch experiments:

Results from the double-notched four-point bend tests, which were used to detect the precursor microstructural cracking events prior to macroscopic fracture in the bone specimens, are shown fractographically in Figs. 5-8. SEM examination of the region around the unbroken notches clearly indicated that without exception, all precursor cracks formed directly at the notch root (Fig. 6). The extremely small (<5 μm) size of the precursor cracks that are imaged (e.g., Fig. 6b where micron-size cracks can be seen directly at the notch root surface) leaves little doubt that crack initiation is *at* the notch and not ahead of it, i.e., that crack initiation occurs in the location of peak strain. Some idea of the corresponding location of the peak stresses can be estimated from Griffiths and Owen's finite-element analysis of the notched-bend bar (Griffiths and Owen, 1971). For the bend specimens tested with a nominal elastic bending stress, σ_{11}, at the notch tip in the 40-100 MPa range ($\sigma_{11}/\sigma_y \sim 0.5$-$1.3$) at maximum load, the maximum tensile stress occurs at roughly 100 to 360 μm ahead of the notch tip, i.e., at a distance of ~0.5 to 1.2 times the notch root radius, assuming pressure-independent yielding. Similar estimates were obtained from the numerical computations

performed in the current work (described in the Appendix), where the peak stresses were found to occur ahead of the notch root at distances of ~0.5 to 1.3 times the notch root radius, depending upon whether a pressure-sensitive "microcracking" or pressure-insensitive "plasticity" model was used. As absolutely no evidence of precursor cracking was found in these regions and all cracking was detected exactly at the notch root, the experimental evidence obtained strongly suggests that fracture in human cortical bone is indeed locally strain-controlled.

3.2 Crack-microstructure interactions and fractography:

From the optical micrographs in Fig. 5, it is evident that the underlying microstructure has a marked influence on the nature of the crack path in human cortical bone. This is particularly evident for the transverse orientation. Whereas fracture in the longitudinal orientations (Figs. 5a,b) nominally follows an expected trajectory dictated by the path of maximum tensile stresses, i.e., a $K_{II} = 0$ path (where K_{II} is the mode II stress intensity), cracks in the transverse orientation can be seen to extend initially in an unlikely direction perpendicular to the notch (Figs. 5c,d). This is further apparent in Fig. 6c, where such microcracks can be seen to initiate well behind the notch root in a direction again normal to that dictated by the path of maximum tensile stress.

SEM micrographs of the subsequent propagation of such cracks and their interaction with the salient microstructural features are shown in Fig. 7. Fig. 7a shows a relatively long crack (~1 mm) in the anti-plane longitudinal orientation. The crack path at this magnification is relatively deflection-free, indicating that the most recognizable feature of the microstructure, the Haversian canals with their concentric lamellar rings, do not play a major role in influencing the crack path, i.e., they neither "attract" nor "repel" a growing crack.

However, several other crack/microstructural interactions mechanisms are evident, which can lead to sources of toughening in bone. Investigation of the near-tip region of this same crack, shown by the black circle in Fig. 7a**,** revealed evidence of so-called *uncracked-ligament bridging*, as indicated by the black arrows in Fig. 7b. This is an extrinsic toughening mechanism involving two-dimensional uncracked regions along the crack path that can bridge the crack on opening; it is commonly seen in metal-matrix composites (Shang and Ritchie, 1989) and intermetallics such as γ-based TiAl titanium aluminide intermetallics (Campbell et al., 1999). Similar bridging, which is often the result of the non-uniform advance of the crack front, is also evident for shorter cracks; typical examples are shown in Figs. 7c and 7d. Uncracked ligament bridging can also be seen in the in-plane longitudinal orientation, as shown by the white arrow in Fig. 7f; *microcracking* is also apparent in the vicinity of the crack in this micrograph. The microcracking can also lead to extrinsic toughening through its effect in creating dilation and reducing the modulus in the region surrounding the crack. For the anti-plane longitudinal orientation, another potential mechanism of toughening in bone can be seen in the form of crack bridging by the collagen fibrils (Fig. 7e).

However, the largest influence of the underlying microstructure on the crack path can be seen in the transverse orientation, where the secondary osteons run along the specimen length (Fig. 3). As mentioned previously, crack initiation and initial crack growth out of the notch was not in the direction normal to the maximum tensile stress, but rather perpendicular to this in the nominal direction of the osteon system (Fig. 6c). As suggested elsewhere (Yeni and Norman, 2000), it would appear that the osteonal cement lines, that are the interface between the osteonal system and the surrounding matrix, provide a weak path for the

propagation of the crack, as shown in Fig. 7g. Indeed, although there is significant cracking ahead of the notch at a Haversian canal (indicated by black arrow), this seems to be totally ignored by the main crack at the notch. However, the marked deflections in crack path seen in this case can lead to substantial toughening and may be the major factor in explaining the anisotropy in the fracture properties in human bone, as discussed below.

Corresponding low and high magnification scanning electron micrographs of the fracture surfaces obtained for the various orientations are shown in Fig. 8. The roughness of the fracture surface, which invariably correlates directly with the toughness, is clearly far greater in the transverse orientation, consistent with the more extensive crack path deflections in this orientation. Also apparent is the occurrence of microcracks which initiate at the various void-like features, e.g., Haversian canals, osteocyte lacunae, etc., in the microstructure of the bone. Fig. 7g and 8g provide examples of microcracks formed at, respectively, a Haversian canal and a lacuna (microcracks indicated by the black arrows), both images illustrating how these void-like microstructural features can act as local stress concentrators.

3.3 Fracture-toughness results:

The fracture toughness, K_c and work of fracture, W_f, values obtained in this study for various specimen orientations are given in Table I and Fig. 9. In terms of the fracture toughness values, the transverse orientation is between 51% and 140% tougher than the longitudinal orientations. However, since the K_c values in the transverse orientation may be somewhat questionable due to the significant crack-path deviations, work of fracture measurements, representing work per unit area needed to generate new crack surface, are also shown and indicate a toughness in the transverse orientation that is again far in excess of the

corresponding values for either the in-plane or anti-plane longitudinal orientations. Since the work of fracture is geometry- and sample-size dependent, it is difficult to compare these latter values with previous measurements, although similar qualitative trends have been previously reported (Lucksanambool et al., 2001).

Such *measured* anisotropy in the toughness of bone is believed to be a direct result of the various toughening mechanisms described above (Section 4.2), namely crack bridging, crack deflection and microcracking. While such mechanisms have long been hypothesised in bone (e.g., Vashishth, 2000; Parsamian and Norman, 2001; Vashishth et al., 2000; Yeni and Fyhrie, 2001), experimental and/or theoretical evidence of their existence, and quantitative relevance, has largely been lacking. This issue is addressed in the following sections.

3.4 Crack-bridging results:

Although the micrographs in the present work (Fig. 7b-f) strongly suggest the presence of crack bridging as a viable toughening mechanism in bone, this alone is not definitive proof. To provide verification of a bridging effect, measurements of the elastic compliance (inverse stiffness) of the cracked specimen were compared in the present study to those made after subsequent machining out the wake of the crack (which removes the bridging elements). The latter measurements were then verified by showing that they were identical to the theoretical compliance of a traction-free crack of the same size. Such procedures have been documented as a means of quantifying the role of such crack bridging in ceramic materials (Kruzic et al., 2003). Results for the anti-plane longitudinal orientation are shown in Fig. 9 and clearly indicate that the crack in the specimen has a lower compliance than a traction-free crack of identical length. Such results provide definitive proof that cracks in human bone are bridged.

Such measurements also permit the approximate quantification of the effect of such bridging on the toughening of bone from the difference between the two curves at maximum load; this gives the additional load sustained at the load-line, P_{br} ~1.5 N, to overcome the effect of the "bridges" (Ritchie et al., 1989). For the present geometry, this value of the bridging load, P_{br}, can be equated to a bridging stress intensity, K_{br}, using Eq. 1. Calculations of K_{br}, which represent an extrinsic contribution to the fracture toughness, yielded values of ~0.5 MPa√m, i.e., they provide an approximately 25% elevation in K_c for this orientation.

4. Discussion

The microstructure of a material can influence the fracture toughness in two primary ways (Ritchie, 1988; Ritchie, 1999):

(1) it can affect the inherent resistance of the material to microstructural damage and fracture *ahead* of the crack tip, which is termed *intrinsic toughening*, and/or

(2) it can promote crack-tip shielding, i.e., act to reduce the local stress intensity actually experienced *at or behind* the crack tip, which is termed *extrinsic toughening*.

Crack propagation can be considered as a mutual competition between these two classes of mechanisms, i.e., microstructural damage in the process zone ahead of the crack tip, which acts to promote crack extension, and extrinsic crack-tip shielding behind the tip, which acts to impede crack growth. Whereas intrinsic toughening tends to dominate in ductile materials, extrinsic mechanisms are generally the main source of toughening in brittle materials and in many structural composites. Given the relatively brittle nature of bone and the nature of the crack-microstructure interactions described in Section 4.2 above, extrinsic mechanisms appear to provide the principal contributions to the toughness of bone, akin to other mineralized tissue such as dentin (Nalla et al., 2003(3)).

Firstly, in terms of intrinsic damage, we have shown, in this and our previous study (Nalla et al., 2003(1)), what is believed to be the first direct experimental evidence that fracture in human cortical bone is consistent with a *strain-based* criterion, which has been so widely used in theoretical models of the mechanical behavior of bone (Keaveny et al., 1994; Ford and Keaveny, 1996; Yeh and Keaveny, 2001).

Secondly, in terms of the salient toughening mechanisms in bone, it is apparent from the current observations of the crack path with respect to the microstructure that this toughening arises extrinsically from several sources:

- crack bridging by uncracked ligaments
- crack bridging by intact collagen fibrils
- macroscopic crack deflection
- microcracking.

Since the potency of these mechanisms depends on specific microstructural features, which in turn vary with orientation, the marked anisotropy in the fracture toughness of bone can be considered to result directly from the relative contributions of these mechanisms.

The influence of the microstructure of bone is strongest for the cracks growing transversely. This is believed to be the result of the so-called cement lines (the bone-matrix interface) offering a path of lower resistance to such cracks. For cracks growing longitudinally, the osteons do not seem to influence the macroscopic crack growth substantially (Fig. 7a). This is reflected in the measured fracture toughness results, which also display a marked orientation-dependence. The fracture toughness values of 2-6 MPa√m that were obtained (Table I, Fig. 9) are consistent with previous results that give the toughness of bone to be in the 2-8 MPa√m range (Zioupos and Currey (1998);

Lucksanambool et al., 2001; Phleps et al., 2000), and to be higher in the transverse direction (Lucksanambool et al., 2001; Phleps et al., 2000; Behiri and Bonfield, 1989). It is believed that this variation in toughness with orientation results directly from how the crack interacts with the salient microstructural features, which in turns dictates the toughening mechanisms involved. Indeed, our detailed microscopic observations suggest that a number of such toughening mechanisms are active, including bridging by uncracked ligaments and by collagen fibers, (damage zone) crack deflection, and microcracking.

The highest toughness was observed in the transverse orientation where the crack path deflects at almost 90° to the plane of maximum tensile stress (Figs. 5c, 5d, 6c, 7g and 8e). The effect of this deflection is to significantly increase the toughness, as shown by the following analysis. Assuming for the sake of simplicity that these deflections/kinks represent in-plane tilts through an angle α to the crack plane, then the local mode I and mode II stress intensities, k_1 and k_2, at the deflected crack tip will be given by (Bilby et al., 1978; Cottrell and Rice, 1980):

$$k_1(\alpha) = c_{11}(\alpha)\, K_I + c_{12}(\alpha)\, K_{II} \ ,$$

$$k_2(\alpha) = c_{21}(\alpha)\, K_I + c_{22}(\alpha)\, K_{II} \ , \qquad (4)$$

where K_I (5.33 MPa$\sqrt{m}$) and K_{II} (= 0) are, respectively, the mode I and mode II global (applied) stress intensities for a main crack, and the coefficients, $c_{ij}(\alpha)$, are mathematical functions of the deflection angle, α (~90°) (Bilby et al., 1978; Cottrell and Rice, 1980). The effective stress intensity at the tip of the deflected crack tip, K_d, can then be calculated by summing the mode I and mode II contributions in terms of the strain-energy release rate, viz:

$$K_d = (k_1^2 + k_2^2)^{1/2} \ , \qquad (5)$$

which suggests that the value of the stress intensity at the crack tip is reduced locally by some 50% due to such deflection to ~2.7 MPa√m, as compared to that for an undeflected crack. This calculation is consistent with the toughness being approximately twice as high in this orientation as compared to the longitudinaly orientations (Table I).

A toughening effect is also seen in the anti-plane longitudinal orientation where crack bridging by uncracked ligaments (and collagen fibrils) is apparent (Figs. 7a-7e). In the present study, for the first time the magnitude of such bridging has been quantitatively evaluated by experiment; as described in Section 4.4, a small, but finite, contribution of ~0.5 MPa√m was estimated experimentally using compliance-based measurements for this toughening mechanism (Section 4.4).

It is not possible experimentally to separate out the relative contributions to bridging from the uncracked ligaments or the collagen fibrils. However, this distinction can be deduced from theoretical models for the two bridging mechanisms. Theoretical estimates of ligament bridging can be made based on a limiting crack-opening approach (Shang and Ritchie, 1989):

$$K_{br} = - f_{ul} K_I [(1 + l_{ul} /rb)^{1/2} -1] / [1 - f_{ul} + f_{ul} (1 + l_{ul} /rb)^{1/2}] \ , \qquad (3)$$

where f_{ul} is the area fraction of bridging ligaments on the crack plane (~0.2-0.4, from crack path observations), K_I is the applied (far-field) stress intensity (2.4 MPa√m), l_{ul} is the bridging zone size (~50-300 μm, from crack path observations), r is a rotational factor (0.20-0.47) and b is the length of the remaining uncracked region ahead of the crack. Again, substituting typical values for these parameters, toughening of the order of K_{br} ~ 0.3 MPa√m was obtained. For toughening associated with bridging by the collagen fibrils, the uniform

traction Dugdale zone model (Evans and McMeeking, 1986) can be employed to obtain an estimate of the resulting decrease in the stress intensity, K_b^f, due to "fiber bridging", viz:

$$K_b^f = 2\,\sigma_b f_f\,(2\,l_f\,/\,\pi)^{1/2}\ , \tag{4}$$

where σ_b is the normal bridging stress on the fibrils (~ 100 MPa), f_f is the effective area fraction of the collagen fibrils active on the crack plane (~0.15, from crack path observations), and l_f is the bridging zone length (~10 μm, from crack path observations). Using these estimates of the parameters in Eq. 4, a value of K_b^f ~0.07 MPa√m can be obtained. These estimates would suggest that the uncracked ligament bridging provides a far more significant contribution to the toughness of bone than bridging by individual collagen fibers.

In summary, direct experimental evidence has been presented in support of a *strain-controlled* fracture mechanism in bone. In addition, a series of extrinsic toughening mechanisms in bone have been identified (including crack bridging by uncracked ligaments and collagen fibrils, crack deflection, and microcracking), based on observations of the interaction of the crack path with the underlying microstructure. Based on these observations, experimental compliance measurements, and theoretical estimates for the toughening contributions of the mechanisms, the anisotropy in the fracture toughness of bone with orientation can be understood; specifically, we find a smaller (but finite) contribution to the toughening in the (anti-plane) longitudinal orientation due to crack bridging as compared to the larger contribution from crack deflection in the transverse orientation. It is believed that the results presented here are critical steps to the understanding of structure-function relationships in bone and can form the basis for a physically-based micro-mechanistic

understanding of the fracture and failure of human cortical bone from a fracture-mechanics perspective.

Acknowledgments

This work was supported in part by the National Institutes of Health under Grant No. P01DE09859 (for RKN) and by the Livermore Science and Technology Office (LSTO) under the auspices of the US Department of Energy Contract No. W-7405-Eng48 (for JHK). The authors wish to thank Dr. C. M. Puttlitz (Department of Orthopedic Surgery, University of California, San Francisco, CA, U.S.A.) for supply of the human cortical bone used in this study, Dr. J. J. Kruzic (Materials Science Division, Lawrence Berkeley National Laboratory, Berkeley, CA, U.S.A.) for help with the compliance measurements and for many useful discussions, and Dr. S. J. Marshall (Department of Preventive and Restorative Dental Sciences, University of California, San Francisco, CA, U.S.A.) for her continued support and encouragement.

References

An, Y.H., 2000. Mechanical properties of bone. In: Mechanical testing of bone and the bone-implant interface. CRC Press, Boca Raton, pp. 41-63.

Ashman, R.B., Rho, J.Y., 1988. Elastic modulus of trabecular bone material. J Biomech 21, 177-181.

ASTM E 399-90 (Reapproved 1997), 2001. Annual Book of ASTM Standards, Vol. 03.01: Metals- Mechanical testing; Elevated and low-temperature tests; Metallography. ASTM, West Conshohocken.

Behiri, J.C., Bonfield, W., 1989. Orientation dependence on fracture mechanics of bone. J Biomech 22, 863-872.

Bilby, B.A., Cardew, G.E., Howard, I.C., 1978. Stress intensity factors at the tips of kinked and forked cracks. In: Fracture 1977, Vol. 3. Pergamon Press, Oxford, pp. 197-200.

Burnstein, A.H., Reilley, D.T., Martens, M., 1976. Ageing of bone tissue: Mechanical properties. J Bone Joint Surg 58A, 82-86.

Burr, D.B., 2002. The contribution of the organic matrix to bone's material properties. Bone 31, 8-11.

Campbell, J.P., Venkateswara Rao, K.T., Ritchie, R.O., 1999. The effect of microstructure on fracture toughness and fatigue crack growth behaviour in γ-titanium aluminide based intermetallics. Metall Mater Trans A 30A, 563-577.

Cotterell, B., Rice, J.R., 1980. Slightly curved or kinked cracks. Int J Fract 16, 155-169.

Currey, J.D., 1970. The mechanical properties of bone. Clin Orthop 73, 209-231.

Evans, A.G., McMeeking, R.M., 1986. On the toughening of ceramics by strong reinforcements. Acta Metall 34, 2435-2441.

Ford, C.M., Keaveny, T.M., 1996. The dependence of shear failure properties of trabecular bone on apparent density and trabecular orientation. J Biomech 29, 1309-1317.

Govindjee, S., Kay, G.J., Simo, J.C., 1995. Anisotropic modelling and numerical simulation of brittle damage in concrete. Int J Numerical Methods in Engineering 38, 3611-3633.

Griffiths, J.R., Owen, D.R.J., 1971. An elastic-plastic stress analysis for a notched bar in plane strain bending. J Mech Phys Solids 19, 419-431.

Haggag, F.M., Underwood, J.H., 1984. Compliance of a three-point bend specimen at load line. Int J Fract 26, R63-R65.

Hill, R., 1950. The Mathematical Theory of Plasticity. Clarendon Press, Oxford.

Imbeni, V., Nalla, R.K., Bosi, C., Kinney, J.H., Ritchie, R.O., 2003. On the *in vitro* fracture toughness of human dentin. J Biomed Mater Res. in press.

Katz, J.L., 1980. The structure and biomechanics of bone. Symp Soc Exp Biol 34, 137-168.

Keaveny, T.M., Borchers, R.E., Gibson, L.J., Hayes, W.C., 1993. Theoretical analysis of the experimental artifact in trabecular bone compressive modulus. J Biomech 26, 599-607.

Keaveny, T.M., Wachtel, E.F., Ford, C.M., Hayes, W.C., 1994. Differences between the tensile and compressive strengths of bovine tibial trabecular bone depends on modulus. J Biomech 27, 1137-1146.

Kruzic, J.J., Cannon, R.M., Ritchie, R.O., 2003. Fatigue-crack growth behavior of short cracks in polycrystalline alumina: Quantification of the role of grain bridging. J Am Ceramic Soc. in review.

Lindahl, O., Lindgren, A.G., 1967. Cortical bone in man. I. Variation of the amount and density with age and sex. Acta Orthop Scand 38, 133-140.

Lotz, J.C., Cheal, E.J., Hayes, W.C., 1991. Fracture prediction for the proximal femur using finite element models: Part I-Linear analysis. J Biomech Eng 113, 353-360.

Lucksanambool, P., Higgs, W.A.J., Higgs, R.J.E.D., Swain, M.W., 2001 Fracture toughness of bovine bone: influence of orientation and storage media. Biomater 22, 3127-3132.

Maker, B.N., and Hallquist, J.O., 1995. NIKE-3D - A nonlinear, implicit, three-dimensional finite element code for solid and structural mechanics-user's manual, UCRL-MA-105268-REV-1. Lawrence Livermore National Laboratory, Livermore.

McClintock, F.A. 1958. J Appl Mech Trans ASME Ser H 25, 363.

Nalla, R.K., Kinney, J.H., Ritchie, R.O., 2003(1). Mechanistic Fracture Criteria for the Failure of Human Cortical Bone. Nature Mater. in press (Feb. issue).

Nalla, R.K., Kinney, J.H., Ritchie, R.O., 2003(2). On the fracture of human dentin: Is it stress- or strain-controlled. J Biomed Mater Res. in review.

Nalla, R.K., Kinney, J.H., Ritchie, R.O., 2003(3). Effect of orientation on the *in vitro* fracture toughness of dentin: The role of toughening mechanisms. Biomater. in review.

Niebur, G.L., Feldstein, M.J., Yuen, J.C., Chen, T.J., Keaveny, T.M., 2000. High-resolution finite element models with tissue strength asymmetry accurately predict failure of trabecular bone. J Biomech 33, 1575-1583.

Orowan, E., 1948-9. Fracture and strength of solids. Rep Progr Phys 12, 185-232.

Park, J.B., Lakes, R.S., 1992. Biomaterials: An Introduction. Plenum Press, New York.

Parsamian, G.P., Norman, T.L., 2001. Diffuse damage accumulation in the fracture process zone of human cortical bone specimens and its influence on fracture toughness. J Mater Sci: Mater Med 12, 779-783.

Phelps, J.B., Hubbard, G.B., Wang, X., Agrawal, C.M., 2000. Microstructural heterogeneity and the fracture toughness of bone. J Biomed Mater Res 51, 735-741.

Ritchie, R.O., Knott, J.F., Rice, J.R., 1973. On the relationship between critical tensile stress and fracture toughness in mild steel. J Mech Phys Solids 21, 395-410.

Ritchie, R.O., Thompson, A.W., 1985. On macroscopic and microscopic analyses for crack initiation and crack growth toughness in ductile alloys. Metall Trans A 16A, 233-248.

Ritchie, R.O., 1988. Mechanisms of fatigue crack propagation in metals, ceramics and composites: Role of crack-tip shielding. Mater Sci Eng 103, 15-28.

Ritchie, R.O., Yu, W., Bucci, R.J., 1989. Fatigue crack propagation in ARALL laminates: Measurement of the effect of crack-tip shielding from crack bridging. Eng Fract Mech 32, 361-377.

Ritchie, R.O. 1999. Mechanisms of fatigue-crack propagation in ductile and brittle solids. Int J Fract 100, 55-83.

Shang, J.H., Ritchie, R.O., 1989 Crack bridging by uncracked ligaments during fatigue-crack growth in SiC-reinforced aluminum-alloy composites. Metall Trans A 20A, 897-908.

Simo, J.C., Ju, J.W., 1987. Strain- and stress-based continuum damage models-I. Formulation. Int J Solids and Structures 23, 821-840.

Thompson, J.B., Kindt, J.H., Drake, B., Hansma, H.G., Morse, D.E., Hansma, P.K., 2001. Bone indentation recovery time correlates with bond reforming time. Nature 414, 773-776.

Vashishth, D., Behiri, J.C., Bonfield, W., 1997. Crack growth resistance in cortical bone: Concept of microcrack toughening. J Biomech 30, 763-769.

Vashishth, D., 2000. In vivo diffuse damage in human vertebral trabecular bone. Bone 26, 147-152.

Vashishth, D., Tanner, K.E., Bonfield, W., 2000. Contribution, development and morphology of microcracking in cortical bone during crack propagation. J Biomech 33, 1169-1174.

Wang, X., Bank, R.A., Tekoppele, J.M., Agrawal, C.M., 2001. The role of collagen in determining bone mechanical properties. J Orthop Res 19, 1021-1026.

Wang, X., Shen, X., Li, X., Agrawal, C.M., 2002. Age-related changes in the collagen network and the toughness of bone. Bone 31, 1-7.

Wright, T.M., Hayes, W.C., 1976. The fracture mechanics of fatigue crack propagation in compact bone. J Biomed Mater Res 10, 637-648.

Yeh, O.C., Keaveny, T.M., 2001 Relative roles of microdamage and microfracture in the mechanical behavior of trabecular bone. J Orthop Res 19, 1001-1007.

Yeni, Y.N., Norman, T.L., 2000. Calculation of porosity and osteonal cement line effects on the effective fracture toughness of cortical bone in longitudinal crack growth. J Biomed Mater Res 51, 504-509.

Yeni, Y.N., Fyhrie, D.P., 2001. Collagen-bridged microcrack model for cortical bone tensile strength. In: Proceedings of the 2001 Summer Bioengineering Conference, BED-Vol. 50. ASME, New York, pp 293-294.

Zioupos, P., Currey, J.D., 1998. Changes in the stiffness, strength, and toughness of human cortical bone with age. Bone 22, 57-66.

Zioupos, P., Currey, J.D., Mirza, M.S., Barton, D.C., 1995. Experimentally determined microcracking around a circular hole in a flat plate of bone: Comparison with predicted stresses. Philos Trans R Soc Lond B Biol Sci 347, 383-396.

Appendix

Stress and Strain Distributions Ahead of a Notch in the Presence of Inelasticity

An aim of this paper is the definition of the critical fracture event in bone in terms of either a stress- or strain-based criterion using the double-notch technique. In metallic materials, brittle fracture by cleavage cracking is commonly modeled to be stress-controlled, involving the unstable propagation of a microcrack, initiated when the local tensile stresses exceed a critical local fracture stress (Orowan, 1948). Ahead of a sharp crack or rounded notch, the probability of this first local event occurring is likely to be highest near the location of maximum tensile stress, which in the absence of yielding is *at* the crack or notch tip. However, in the presence of inelastic deformation, there is usually some degree of relaxation of the stresses in the inelastic ("yielded") zone surrounding the notch/crack. This results in the maximum local tensile stresses being located some distance *ahead* of the notch, towards the elastic-inelastic interface (Hill, 1950), and hence the most probable site for the initiation of fracture, moves *ahead* of the tip (Ritchie et al., 1973). The location of this site depends on several factors, including the applied stress intensity K, the elastic modulus E, yield strength σ_y, and, in the case of a notch, its root radius or included angle. For a sharp crack in a (metallic) material undergoing pressure-independent yielding, it is located at roughly two crack-tip opening displacements from the crack tip, i.e., at a distance on the order of $K^2/\sigma_y E$ (see Ritchie and Thompson, 1985); for a rounded notch, it is several orders of magnitude further away from the tip, essentially at, or much closer to, the boundary of the plastic zone, i.e., at a distance on the order of $(K/\sigma_y)^2$ (Hill, 1950; Griffiths and Owen, 1971). Ductile fracture, conversely, has been modeled as locally strain-controlled, in metallic materials typically involving the initiation and coalescence of voids (McClintock, 1958). Ahead of a sharp crack or rounded notch, this event is most likely to occur at the location of maximum equivalent strain, which is at the crack or notch tip (Ritchie and Thompson, 1985). Thus, for materials that display any degree of inelasticity, the location of the microstructural cracking event that precedes macroscopic fracture at a notch is a definitive indicator of

whether the fracture is locally stress- or strain-controlled; strain-controlled fracture will initiate at the notch whereas stress-controlled will initiate ahead of the notch.[1]

Although the notch stress and strain distributions are well known for metals (Hill, 1950; Griffiths and Owen, 1971) displaying pressure-insensitive, shear-driven plasticity (Fig. 1), the corresponding solutions for materials such as bone, where inelasticity may additionally involve pressure-sensitive mechanisms such as microcracking, are not available. Consequently, to derive such distributions, numerical analysis using the nonlinear, implicit, three-dimensional finite-element code NIKE3D (Maker and Hallquist, 1995) was used to simulate inelastic deformation ahead of a notch, which was simply idealized as a hole under uniaxial tensile loading in plane strain. Using symmetry, only one quadrant of the problem was modeled with 4000 linear finite elements in a graded mesh. The region simulated extended over a distance equivalent to 100 times the radius of the hole in both directions. Uniaxial displacement was applied along the upper boundary. Infinite body conditions were approximated by constraining the edge of the region to move with parallel motion.

To simulate deformation by pressure-insensitivity plasticity and pressure-sensitive microcracking, two nonlinear materials models were used. The first "plastic damage" model (PD) was based on the work of Niebur et al., 2000, and used a von Mises yield criterion. Specifically, at stresses beyond the yield stress, the material is allowed to become perfectly plastic; plastic strain is accumulated, and there is no change in the unloading modulus. The isotropic Young's modulus was taken as 18.7 GPa.

The second nonlinear materials model, which was utilized to better simulate deformation by microcracking, was based upon the oriented "brittle-damage" model (BD) described by Govindjee et al., 1995. This model treats the compliance tensor as an internal variable, and adopts the principle of maximum damage dissipation (Simo and Ju, 1987) (equivalent to the principle of maximum plastic work in models of associative plasticity). In compression, the constituent response of the tissue is taken to be plastic yielding (identical to the PD model). In tension, however, a smeared-crack model was used to simulate the effects of damage evolution. This has the effect of reducing the element stiffness in response to an increase in microcrack density, the growth of which is controlled by the fracture toughness. A fracture

[1]It might be noted here that even though the actual measurement of the fracture toughness must involve fracture from a nominally atomically sharp crack, this particular experiment is best carried out with rounded notches as the distinction between the sites of the maximum tensile stress and strain substantially diminishes as the root radius approaches zero.

toughness value of K_c = 3.2 MPa√m (equivalent to a strain-energy release rate of ~500 J/m^2) was selected from the middle of the range of K_c values for bone (Zioupos and Currey, 1998; Lucksanambool et al., 2001; Phleps et al. 2000), consistent with the present results (Table I). As microcracking damage was considered to be unrecoverable, this reduced the unloading modulus. The damage threshold for microcrack nucleation was taken to be a strain of 0.6%.

Results from the finite-element simulations obtained are shown in Fig. A1 in terms of the normalized stress and strain distributions over distance from the notch/hole tip. As is evident, for both the plasticity (PD) and brittle-damage (BD) models, the stresses peak ahead of the notch root; the strains, on the other hand peak at the root and, in fact, decrease monotonically with increasing distance from the root. Thus, both the stress and strain distributions ahead of a notch are qualitatively similar for materials undergoing either classical shear-driven plasticity or pressure-sensitive microcracking.

As an aside, it is interesting to note that although these two fields are qualitatively similar, there is one striking quantitative difference in the normal stress distributions predicted by the pressure-insensitive plasticity (PD) and pressure-sensitive microcracking (BD) models. For plasticity (PD), the normal stress near the notch is everywhere greater than the yield stress and is increasing with the applied load, while for microcracking (BD), it is everywhere less than or equal to the "yield" stress and is decreasing with the applied load. This follows from the pressure insensitivity of the von Mises criteria used in the PD model, which results in a larger normal stress (due to the additional hydrostatic component) required to yield the material. The increase of the hydrostatic component of stress near the notch with increasing load results in a stabilizing effect, in contrast to the BD model that uses a maximum principal stress criteria. In the absence of damage evolution, the normal stress can only reach the "yield" stress and never exceed it. With the evolution of damage, the normal stress carrying capacity of the material is monotonically reduced to zero, resulting in "fracture" at a local level. Since this damage evolution process can be correlated with the development of local strain, it can be interpreted as a local, strain-controlled, fracture mechanism. This fracture process is the end result of the inelastic deformation mechanism (microcracking) being simulated using the BD model; the inelastic deformation naturally evolves pristine material to a damaged state, and finally, to a fractured state (zero load-

carrying capacity). In the PD model, the inelastic deformation mechanism (dislocation motion, polymer chain sliding, etc.) is not as strongly coupled to the fracture mechanism (cleavage crack, particle decohesion/breakage, etc.) but rather facilitates such mechanisms by increasing the normal stress ahead of the notch and accommodating large strains at the notch tip. Therefore, it is important to distinguish between inelastic deformation mechanisms that facilitate local damage processes and eventually lead to fracture, e.g., plasticity, from those inelastic deformation mechanisms that directly cause fracture, e.g., microcracking.

Table I: Measured fracture toughness values as a function of orientation

Orientation	**Fracture toughness** K_c (MPa√m)	**Average** K_c (MPa√m)*	**Work of fracture** W_f (J/m^2)	**Average** W_f (J/m^2)*
Anti-plane Longitudinal	2.42	2.21 (0.18)	617.28	528.26 (62.95)
	2.23		484.26	
	1.97		483.25	
In-plane Longitudinal	3.36	3.53 (0.13)	186.78	295.50 (76.91)
	3.68		352.61	
	3.54		347.12	
Transverse	5.21	5.33 (0.41)	2132.94	2325.41 (152.54)
	5.89		2506.01	
	4.90		2337.28	

* Values in brackets are the standard deviations.

List of Figure Captions

Fig. 1: (a) Tensile stress, σ_{11}, and (b) strain, ε_{11}, distributions ahead of a rounded notch in an elastic-plastic material (Hill, 1950; Griffiths and Owen, 1971). Also shown are schematic illustrations of possible (a) stress-controlled and (b) strain-controlled fracture mechanisms emanating from such notches. Note that for stress-controlled mechanisms, in the presence of any degree of shear-induced inelasticity, the initial fracture event is *ahead* of the notch, essentially at, or behind, the boundary of the plastic zone. For strain-controlled mechanisms, it is *at* the notch root.

Fig. 2: (a) Schematic illustration and (b) optical micrograph of the *double-notched four-point bend test* used to discern whether fracture is stress- or strain-controlled. Between the inner two loading points, the bending moment is constant; thus, when one notch breaks, the other is "frozen" at a point just prior to fracture instability. The region beneath this unbroken notch (as indicated by the encircled area) is then carefully examined to determine the site of the precursor microscopic events involved in the fracture process.

Fig. 3: The various specimen orientations taken from the humerus (with respect to the direction of the osteons, indicated in gray) that were investigated are shown in this illustration.

Fig. 4: (a) Three-point bending configuration utilized for the measurement of the fracture toughness and (b) Optical micrograph of the notch with the fatigue precrack used for these tests.

Fig. 5: Optical micrographs of typical double-notch specimens after fracture. The insets show the orientation of the specimen. A much stronger influence of the underlying microstructure can be seen for the transverse orientations (c and d) as compared to the longitudinal ones (a and b).

Fig. 6: Scanning electron micrographs of the area near the unbroken notch for the orientations investigated. The extremely small (<5 μm) size of the precursor cracks like the one shown in (b) leaves little doubt that crack initiation is *at* the notch and not ahead of it. The stronger influence of the underlying microstructure for the transverse orientation can lead to cracks emanating well behind the notch root, as illustrated in (c). The insets show the orientation of the specimen.

Fig. 7: Scanning electron micrographs illustrating crack-microstructure interactions. For the anti-plane longitudinal orientation, (a) the secondary osteons (indicated by black arrows) have a weak influence on crack path, (b) evidence of uncracked ligament bridging in the encircled region in (a) (indicated by black arrows), (c) further evidence of such bridging due to a secondary lamella, also shown at higher magnification in (d), and (e) possible collagen fibril-based bridging. For the in-plane longitudinal orientation, (f) evidence of uncracked ligament bridging (indicated by black arrow) and extensive microcracking. For the transverse orientation, (g) cracking ahead of the notch at a Haversian canal (indicated by

black arrow), although the actual initiation is at the notch itself, as evidenced by the presence of precursor cracks. The insets show the specimen orientation used and the white arrows in (a)-(f) indicate the direction of nominal crack growth.

Fig. 8: Low (a, c, e) and high (b, d, f, g) magnification scanning electron micrographs of the fracture surfaces. The white arrows show the *nominal* direction of crack propagation. The transverse orientations yield macroscopically rougher fracture surfaces, though the reverse appears to be true on the microscopic level.

Fig. 9: The measured toughness of bone, in terms of (a) fracture toughness and (b) work of fracture results, obtained in this study for different orientations (schematically shown) with respect to the osteons. The half-error bars indicate one standard deviation; the numbers in (a) are the average toughness values.

Fig. 10: Experimental (bridged) and theoretical (traction-free) load-displacement curves (at constant crack length) used to assess the specimen compliance in order to verify the existence of crack bridging in bone. Quantification of the contribution to toughening due to crack bridging can be deduced from the bridging load, P_{br} (see text).

Fig. A1: Non-linear, finite-element computations of the distributions of (a) tensile stress, σ_{11}, and (b) strain, ε_{11}, normalized by the yield stress, σ_y, and yield strain, ε_y, respectively, as a function of distance, x, ahead of a round hole, normalized by the radius of the hole, ρ. Calculations are shown for inelastic deformation based on classical pressure-insensitive, shear-driven plastic deformation (PD) model and pressure-sensitive microcracking (brittle damage - BD) model.

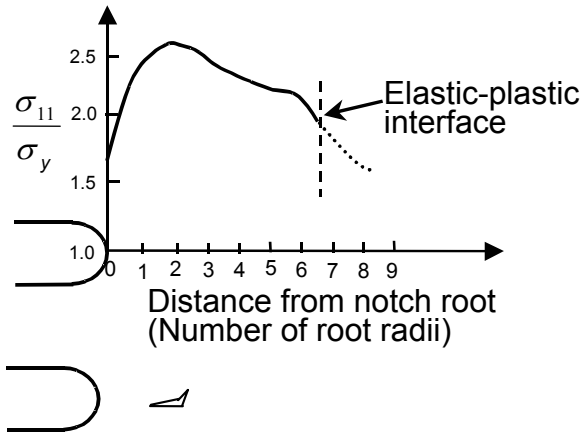

(a)

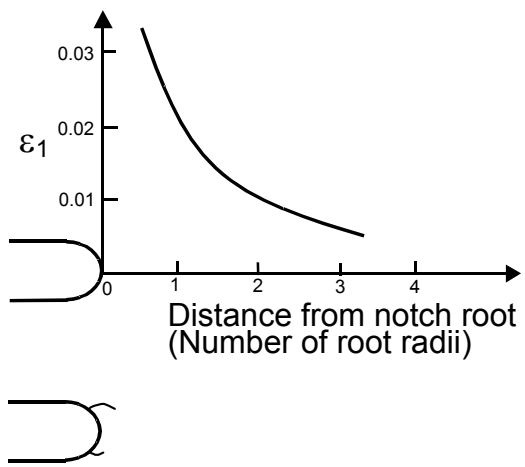

(b)

Fig. 1: (a) Stress and (b) strain distributions ahead of a rounded notch in an elastic-plastic material (Hill, 1950; Griffiths and Owen, 1971). Also shown are schematic illustrations of possible (a) stress-controlled and (b) strain-controlled fracture mechanisms emanating from such notches. Note that for stress-controlled mechanisms, in the presence of any degree of shear-induced inelasticity, the initial fracture event is *ahead* of the notch, essentially at, or just behind, the boundary of the plastic zone. For strain-controlled mechanisms, it is *at* the notch root.

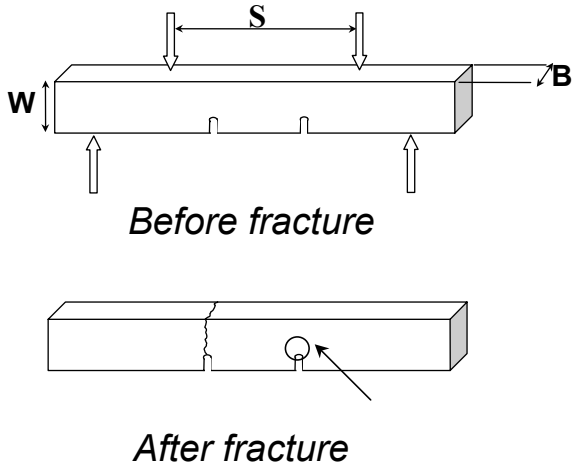

(a)

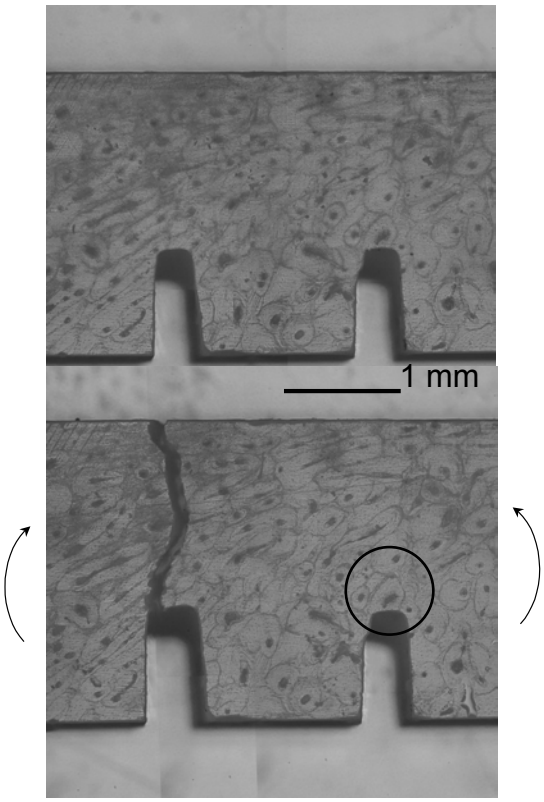

(b)

Fig. 2: (a) Schematic illustration and (b) Optical micrograph of the *double-notched four-point bend test* used to discern whether fracture is stress- or strain-controlled. Between the inner two loading points, the bending moment is constant; thus, when one notch breaks, the other is "frozen" at a point just prior to fracture instability. The region beneath this unbroken notch (as indicated by the encircled area) is then carefully examined to determine the site of the precursor microscopic events involved in the fracture process.

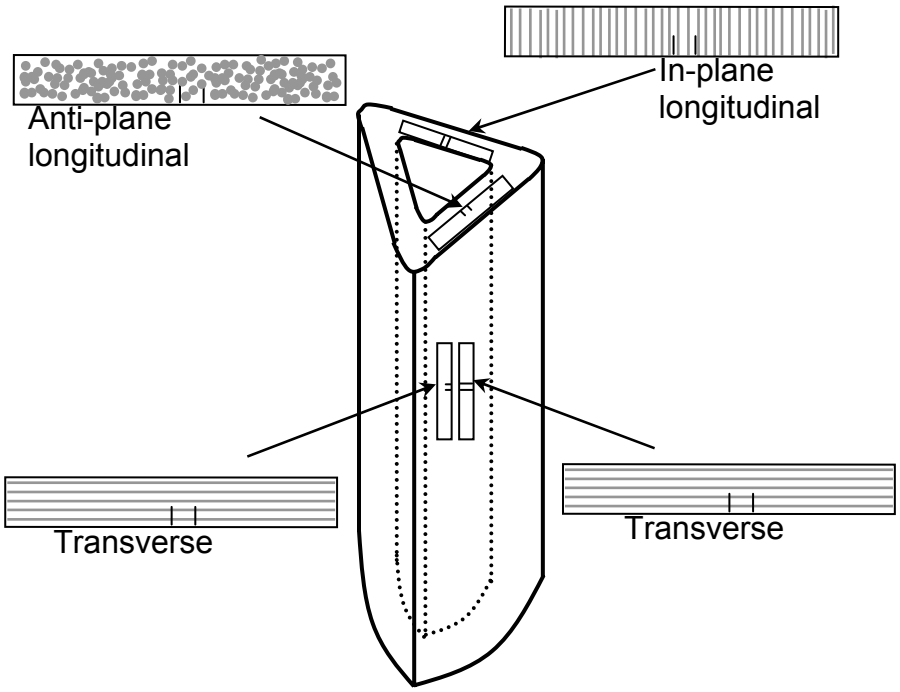

Fig. 3: The various specimen orientations taken from the humerus (with respect to the direction of the osteons, indicated in gray) that were investigated are shown in this illustration.

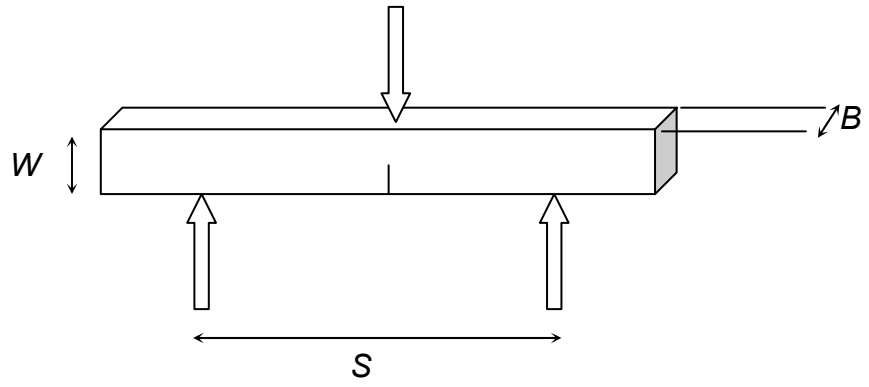

(a)

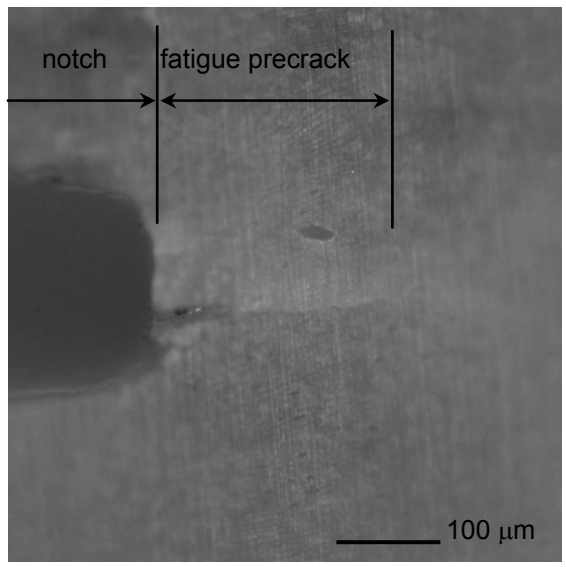

(b)

Fig. 4: (a) Three-point bending configuration utilized for the measurement of the fracture toughness and (b) Optical micrograph of the notch with the fatigue precrack used for these tests.

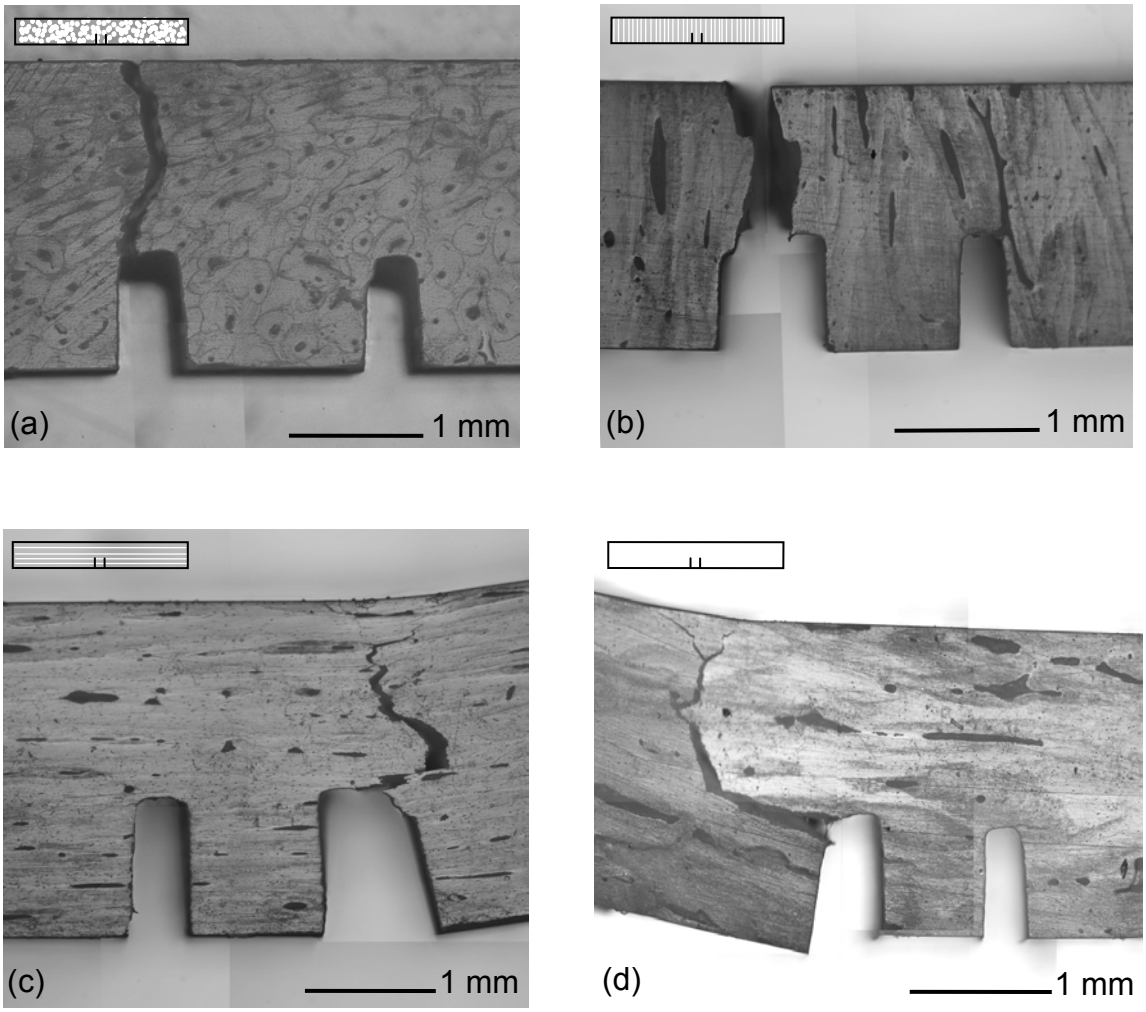

Fig. 5: Optical micrographs of typical double-notch specimens after fracture. The insets show the orientation of the specimen. A much stronger influence of the underlying microstructure can be seen for the transverse orientations (c and d) as compared to the longitudinal ones (a and b).

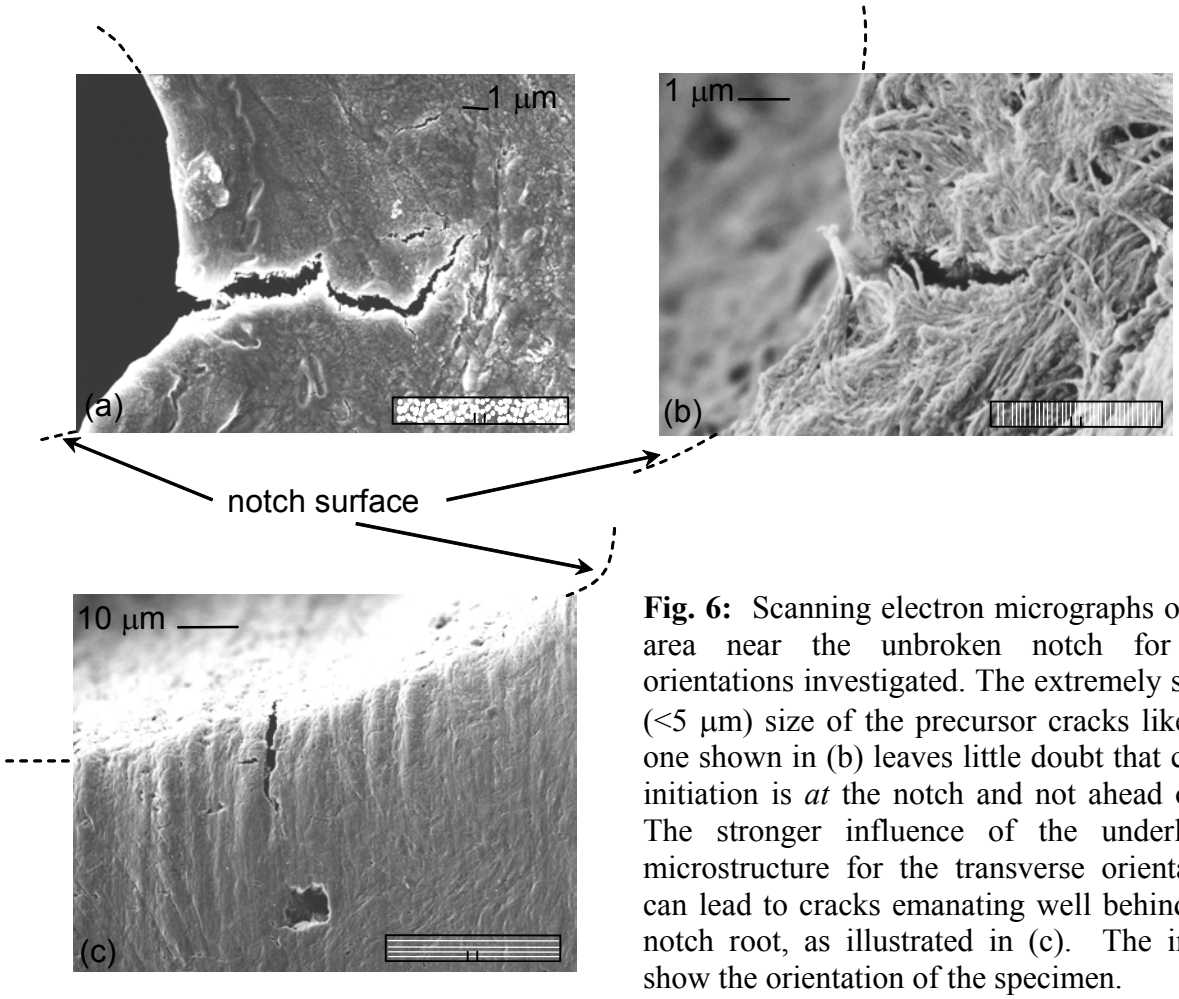

Fig. 6: Scanning electron micrographs of the area near the unbroken notch for the orientations investigated. The extremely small (<5 μm) size of the precursor cracks like the one shown in (b) leaves little doubt that crack initiation is *at* the notch and not ahead of it. The stronger influence of the underlying microstructure for the transverse orientation can lead to cracks emanating well behind the notch root, as illustrated in (c). The insets show the orientation of the specimen.

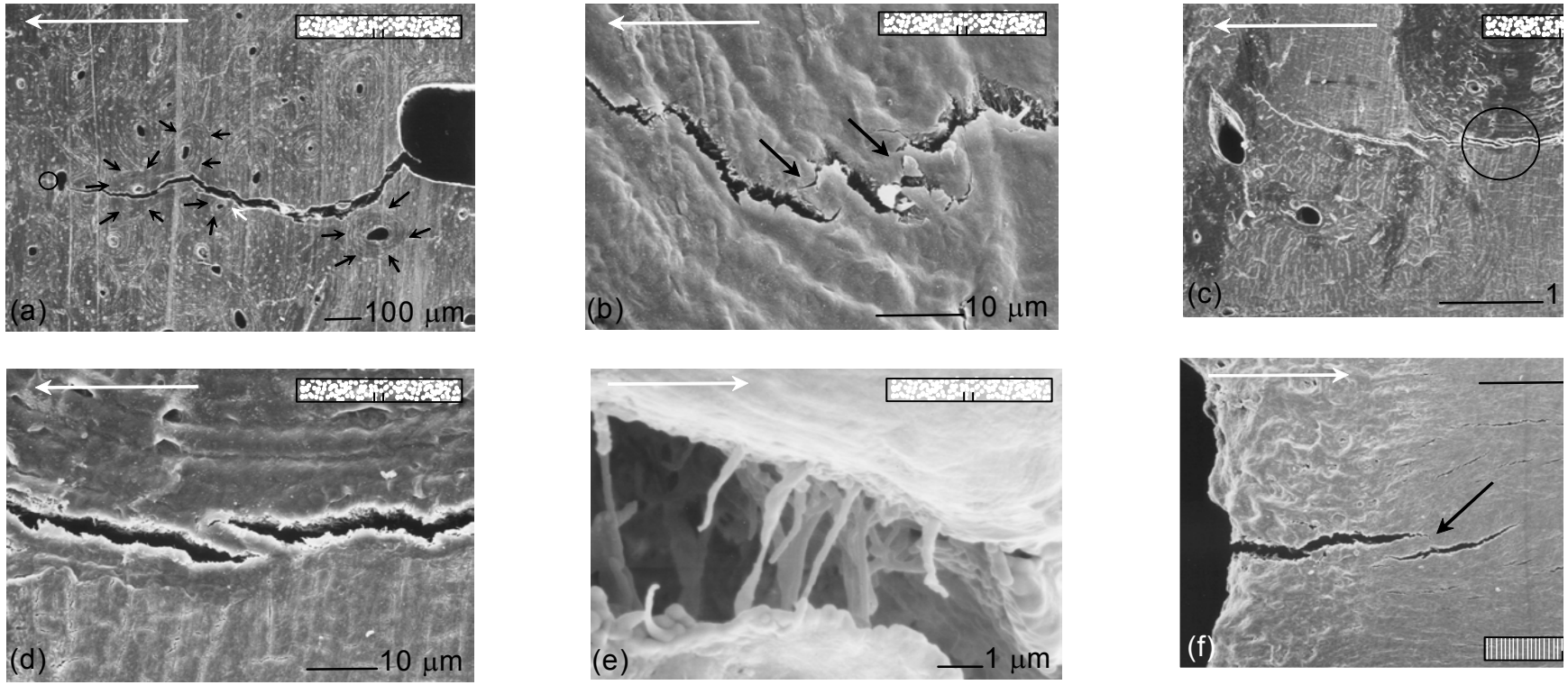

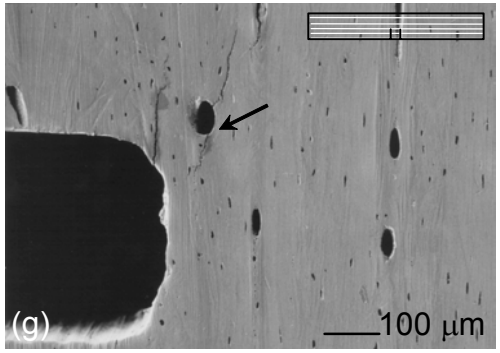

Fig. 7: Scanning electron micrographs illustrating crack-microstructure interactions. For the anti-plane longitudinal orientation, (a) the secondary osteons (indicated by black arrows) have a weak influence on crack path, (b) evidence of uncracked ligament bridging in the encircled region in (a) (indicated by black arrows), (c) further evidence of such bridging due to a secondary lamella, also shown at higher magnification in (d), and (e) possible collagen fibril-based bridging. For the in-plane longitudinal orientation, (f) evidence of uncracked ligament bridging (indicated by black arrow) and extensive microcracking. For the transverse orientation, (g) cracking ahead of the notch at a Haversian canal (indicated by black arrow), although the actual initiation is at the notch itself, as evidenced by the presence of precursor cracks. The insets show the specimen orientation used and the white arrows in (a)-(f) indicate the direction of nominal crack growth.

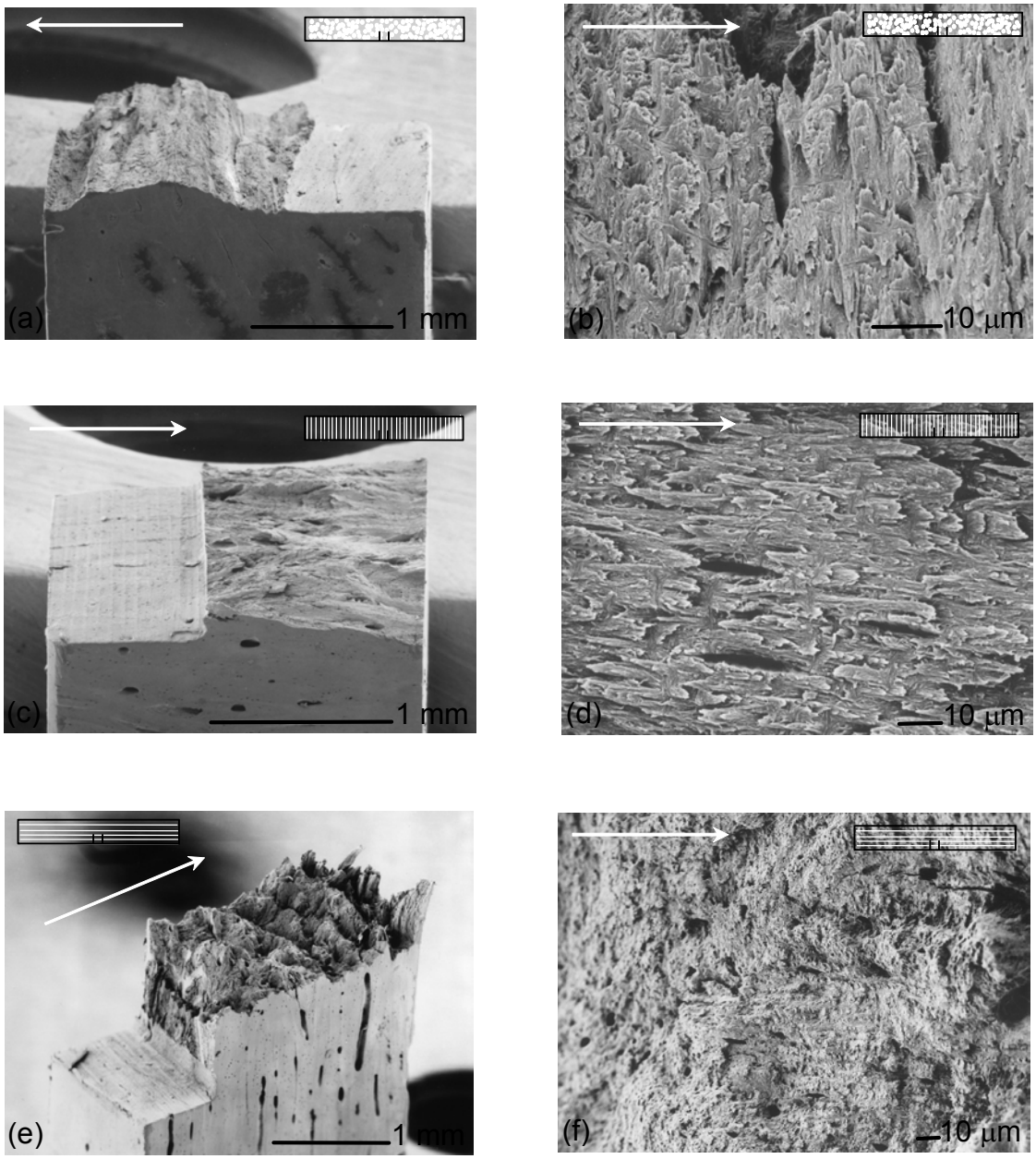

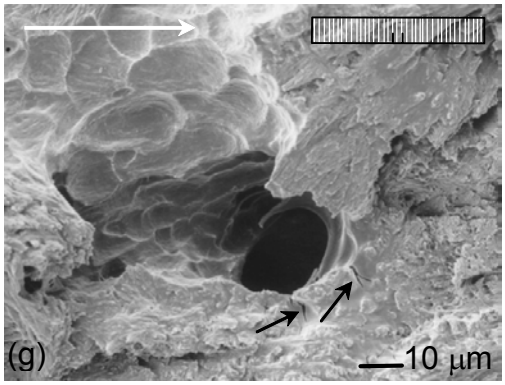

Fig. 8: Low (a, c and e) and high (b, d, f and g) magnification scanning electron micrographs of the fracture surfaces. The white arrows show the *nominal* direction of crack propagation. The transverse orientations yield macroscopically rougher fracture surfaces, though the reverse appears to be true on the microscopic level.

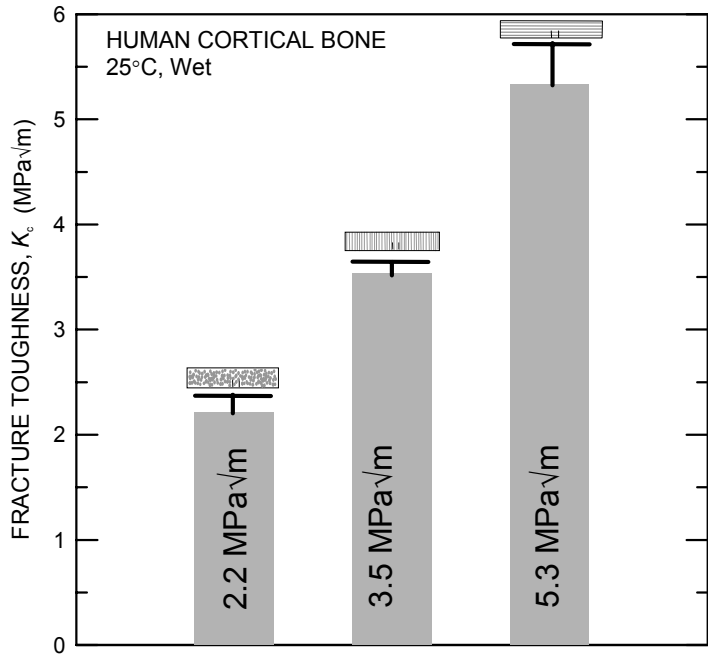

(a)

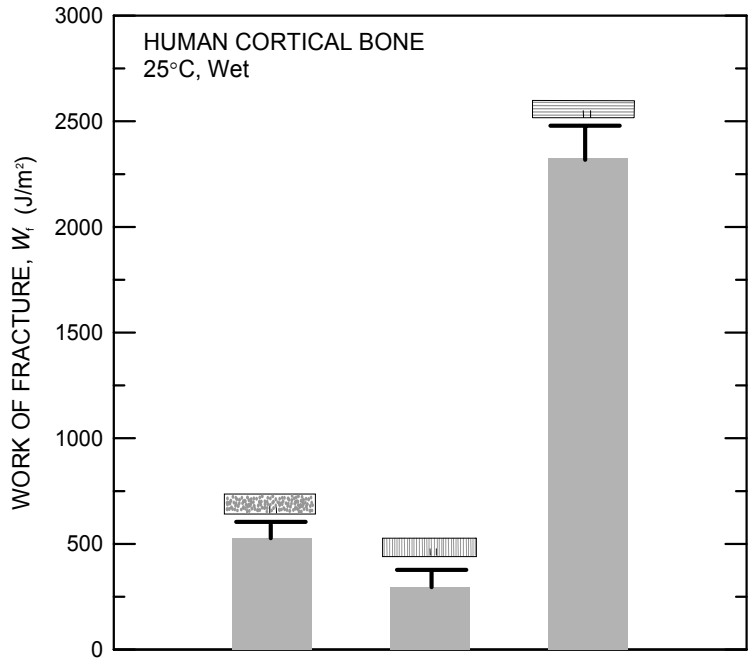

(b)

Fig. 9: The measured toughness of bone, in terms of (a) fracture toughness and (b) work of fracture results, obtained in this study for different orientations (schematically shown) with respect to the osteons. The half-error bars indicate one standard deviation; the numbers in (a) are the average toughness values.

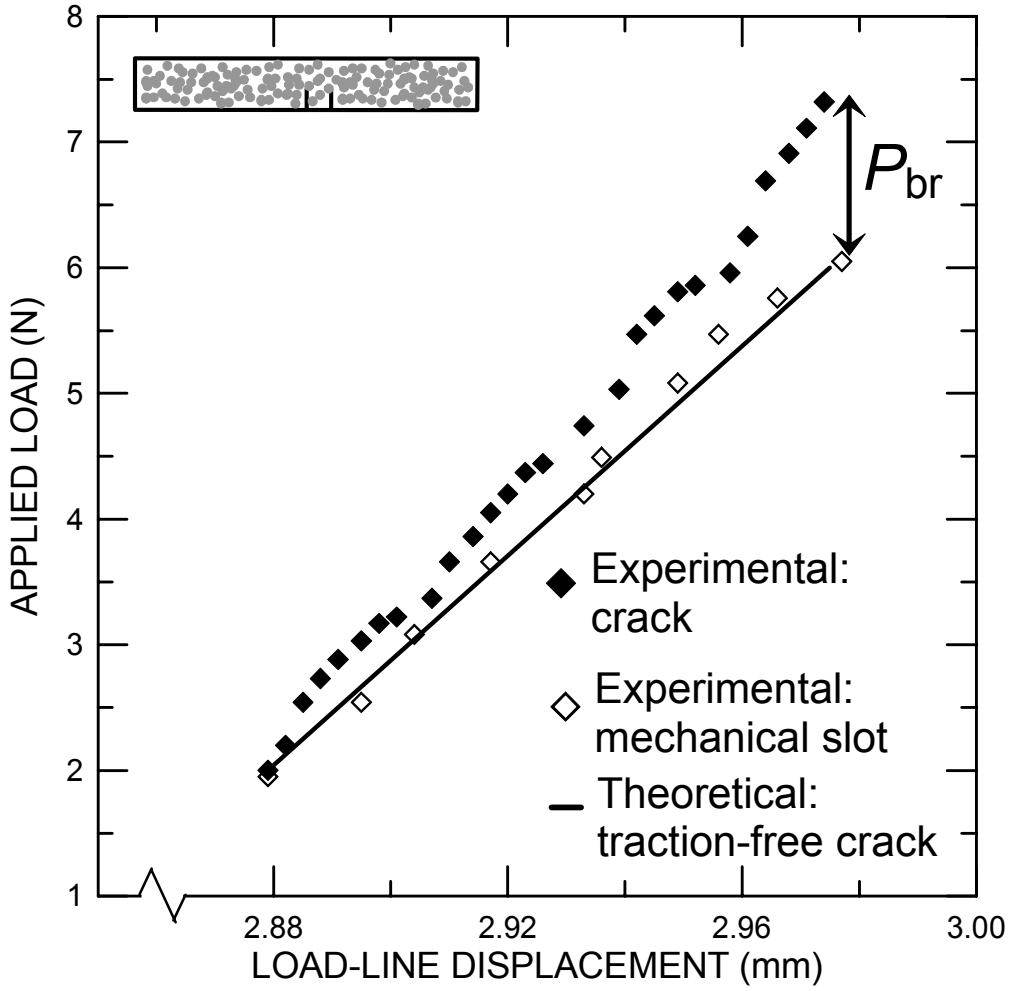

Fig. 10: Experimental (bridged) and theoretical (traction-free) load-displacement curves (at constant crack length) used to assess the specimen compliance in order to verify the existence of crack bridging in bone. Quantification of the contribution to toughening due to crack bridging can be deduced from the bridging load, P_{br} (see text).

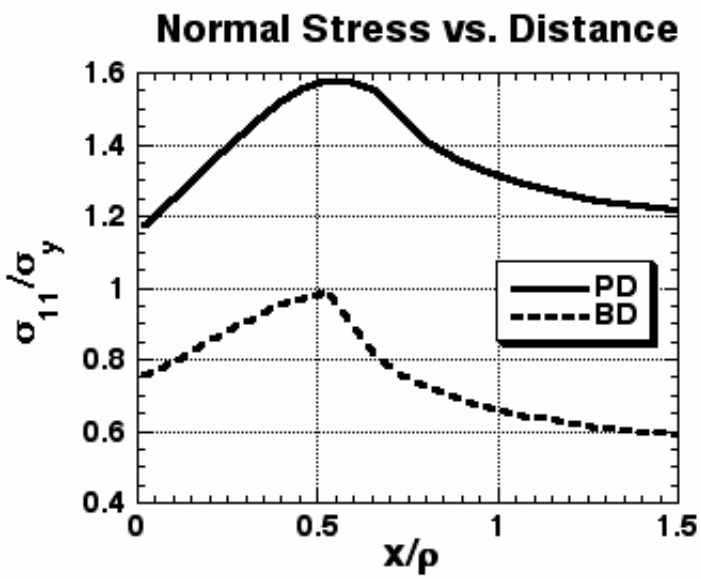

(a)

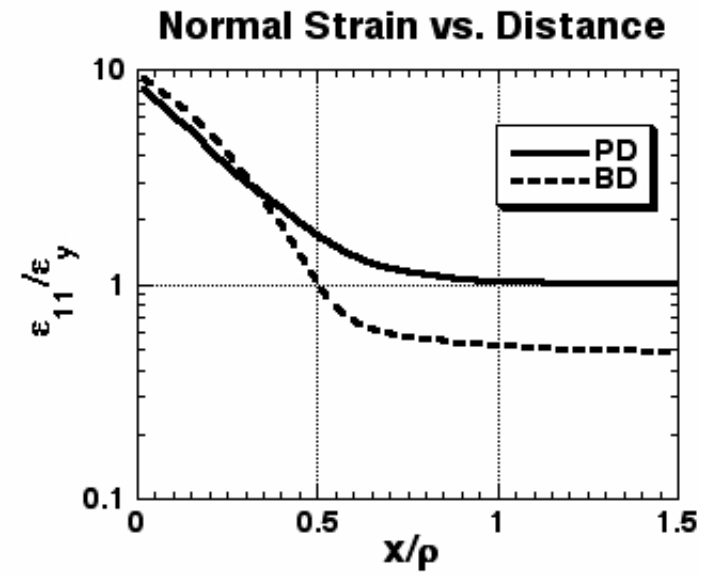

(b)

Fig. A1: Non-linear, finite-element computations of the distributions of (a) tensile stress, σ_{11}, and (b) strain, ε_{11}, normalized by the yield stress, σ_y, and yield strain, ε_y, respectively, as a function of distance, *x*, ahead of a round hole, normalized by the radius of the hole, ρ. Calculations are shown for inelastic deformation based on classical pressure-insensitive, shear-driven plastic deformation (PD) model and pressure-sensitive microcracking (brittle damage - BD) model.